Chapter 14
Size Effects in Cosserat Crystal Plasticity

Samuel Forest and Flavien Ghiglione

Abstract Some Cosserat elastoplasticity models for single crystals are reviewed in the present chapter. Their size-dependent response is evaluated in the case of a simple one-dimensional shear test involving one single slip system and vanishing microrotation prescribed at the boundaries of a material strip of width $2L$. The inhomogeneous distribution of slip in the channel mimics the piling-up of dislocations against the boundaries. The free energy density function depends on the elastic strain and Cosserat curvature tensors. Two types of potentials are examined with respect to the curvature tensor, namely a quadratic function of its norm, on the one hand, and the norm itself, on the second hand. The first model is very often used but turns out to be non-physical since, according to physical metallurgy, the stored energy is proportional to the dislocation density (here the density of geometrically dislocations) rather than its square. The scaling laws predicted by these models are shown to be L^{-2} or L^{-1}, respectively. The latter scaling is reminiscent of Orowan's law of yielding [24]. The chapter ends with the combination of both quadratic and rank one contributions in a unified formulation applied to grain boundary modelling.

Key words: Crystal plasticity · Cosserat elasticity · Cosserat plasticity · Micropolar media · Dislocation density tensor · Dislocation pile-up · Phase field model · Grain boundary

14.1 Introduction

Cosserat modelling has been recognized as a good candidate for continuum modelling of plasticity in crystals due to the relation between inhomogeneous dislocation distributions and lattice curvature [1, 2]. Alternative generalized continuum theories

Samuel Forest · Flavien Ghiglione
Mines Paris PSL University, Centre des Matériaux, CNRS UMR 7633, France,
e-mail: samuel.forest@ensmp.fr, flavien.ghiglione@minesparis.psl.eu

H. Altenbach et al. (eds.), *Sixty Shades of Generalized Continua*,
Advanced Structured Materials 170, https://doi.org/10.1007/978-3-031-26186-2_14

to the Cosserat approach are gradient or micromorphic plasticity, as discussed in [3, 4].

Cosserat crystal plasticity constitutive equations involve elastic contributions, a generalized Schmid law and size–dependent hardening induced by the curvature development, as exposed in the formulations presented in the references [5]-[9]. A critical ingredient of the model is the choice of the dependence of the Helmholtz free energy potential on the curvature tensor. Quadratic dependence has been classically used, especially in strain gradient plasticity models [10, 11]. The quadratic choice was questioned in several contributions like [12, 13], because it predicts unrealistic scaling laws. Alternative potentials include energy functions proportional to the norm of the curvature or dislocation density tensor or its logarithm [14, 15]. Both rank one and logarithmic potentials are non-differentiable at zero curvature which leads to difficulties in implementing these models and requires the consideration of discontinuities in analytical solutions.

To evaluate the various available Cosserat models of elastoplasticity, a simple shear test of a material strip with constrained boundaries is considered, for which analytical solutions can be derived. The microrotation is clamped at the two boundaries, $\theta(-L) = \theta(L) = 0$ and an overall glide amount $\bar{\gamma}$ is applied to the strip. In the following, analytical solutions are provided for quadratic, rank one and combined potentials, considering pure elasticity first, and then crystal plasticity. One single slip system is considered for simplicity and the usual Schmid law is extended to the Cosserat case. In particular the scaling laws with respect to the system size are derived and solutions are compared to existing ones in strain gradient plasticity models involving the dislocation density tensor [15, 16].

In the last section, it is shown that the combined quadratic and rank one potential can be incorporated in a phase field model to describe grain boundary formation in a crystal following [17].

14.2 Problem Setting

14.2.1 Field Equations

Cosserat material points are characterized by their displacement, $\underline{\boldsymbol{u}}$, and microrotation degrees of freedom [18, 19]. The latter microrotation is represented by the axial vector $\underline{\boldsymbol{\theta}}$. Within the small strain, small rotation and small curvature assumption, the Cosserat deformation measures are the relative deformation and curvature tensors defined as

$$\underline{\boldsymbol{e}} = \underline{\boldsymbol{u}} \otimes \boldsymbol{\nabla} + \underline{\underline{\boldsymbol{\epsilon}}} \cdot \underline{\boldsymbol{\theta}}, \quad e_{ij} = u_{i,j} + \epsilon_{ijk}\theta_k \tag{14.1}$$

$$\underline{\underline{\boldsymbol{\kappa}}} = \underline{\boldsymbol{\theta}} \otimes \boldsymbol{\nabla}, \quad \kappa_{ij} = \theta_{i,j} \tag{14.2}$$

in an orthonormal basis.

The conjugate stress quantities to the previous deformation measures are the simple stress tensor, $\underset{\sim}{\boldsymbol{\sigma}}$, and the couple stress tensor, $\underset{\sim}{\boldsymbol{m}}$, which fulfil the static balance laws for momentum and moment of momentum

$$\underset{\sim}{\boldsymbol{\sigma}} \cdot \boldsymbol{\nabla} = 0, \quad \sigma_{ij,j} = 0 \tag{14.3}$$

$$\underset{\sim}{\boldsymbol{m}} \cdot \boldsymbol{\nabla} - \underset{\approx}{\boldsymbol{\epsilon}} : \underset{\sim}{\boldsymbol{\sigma}} = 0, \quad m_{ij,j} - \epsilon_{ijk}\sigma_{jk} = 0 \tag{14.4}$$

in the absence of body forces and couples. These field equations are accompanied by appropriate Neumann boundary conditions in the form

$$\underline{\boldsymbol{t}} = \underset{\sim}{\boldsymbol{\sigma}}.\underline{\boldsymbol{n}}, \quad t_i = \sigma_{ij}n_j, \quad \underline{\underline{\boldsymbol{m}}} = \underset{\sim}{\boldsymbol{m}}.\underline{\boldsymbol{n}}, \quad m_i = m_{ij}n_j \tag{14.5}$$

where $\underline{\boldsymbol{t}}$ and $\underline{\underline{\boldsymbol{m}}}$ are surface traction and couple stress vectors.

14.2.2 Constitutive Equations

The Cosserat deformation tensor is decomposed into elastic and plastic contributions

$$\underset{\sim}{\boldsymbol{e}} = \underset{\sim}{\boldsymbol{e}}^e + \underset{\sim}{\boldsymbol{e}}^p \tag{14.6}$$

In the present work, no such decomposition is introduced for curvature, for the sake of simplicity following [20, 21].

The Helmholtz free energy density function $\psi(\underset{\sim}{\boldsymbol{e}}^e, \underset{\sim}{\boldsymbol{\kappa}})$ is here assumed to depend on elastic deformation and total curvature. Stress–deformation relations are derived from this free energy potential in the form

$$\underset{\sim}{\boldsymbol{\sigma}} = \frac{\partial \psi}{\partial \underset{\sim}{\boldsymbol{e}}^e}, \quad \underset{\sim}{\boldsymbol{m}} = \frac{\partial \psi}{\partial \underset{\sim}{\boldsymbol{\kappa}}} \tag{14.7}$$

Special forms of the free energy function will be considered in the proposed analysis, including a quadratic potential and more general power law potentials.

Crystal plasticity is based on Schmid's yield function, written here for a single slip system

$$f(\underset{\sim}{\boldsymbol{\sigma}}, \underline{\boldsymbol{\ell}}, \underline{\boldsymbol{n}}) = |\tau| - \tau_c, \quad \text{with} \quad \tau = \underset{\sim}{\boldsymbol{\sigma}} : (\underline{\boldsymbol{\ell}} \otimes \underline{\boldsymbol{n}}) \tag{14.8}$$

where τ is the resolved shear stress and τ_c the critical resolved shear stress. The plastic slip system is characterized by the slip direction $\underline{\boldsymbol{\ell}}$ and the normal to the slip plane $\underline{\boldsymbol{n}}$. Normality is a property of the crystal plasticity flow rule

$$\dot{\underset{\sim}{\boldsymbol{e}}}^p = \dot{\gamma} \frac{\partial f}{\partial \underset{\sim}{\boldsymbol{\sigma}}} = \dot{\gamma}\, \underline{\boldsymbol{\ell}} \otimes \underline{\boldsymbol{n}}\ (\operatorname{sign}\tau) \tag{14.9}$$

where $\dot{\gamma}$ is the plastic multiplier.

The Schmid law is generalized here for Cosserat media accounting for generally non-symmetric stress tensor [3]-[5], [9]. A special case limiting the Schmid law to the symmetric part of the stress tensor will also be considered in the following analysis.

14.2.3 Studied Boundary Value Problem

The one-dimensional simple shear problem of Fig. 14.1 is considered successively for several choices of the free energy potential and Schmid law. It involves a single slip system $(\underline{\boldsymbol{\ell}}, \underline{\boldsymbol{n}})$ respectively parallel to the two first vectors of the orthonormal basis $(\underline{\boldsymbol{e}}_1, \underline{\boldsymbol{e}}_2, \underline{\boldsymbol{e}}_3)$. The origin is located at the centre of the strip of width $2L$ and height H. The length H is regarded as infinite so that the solution is invariant along the $y-$direction.

The unknown displacement and microrotation fields takes the simple form:

$$\underline{\boldsymbol{u}} = \bar{\gamma} y \underline{\boldsymbol{e}}_1 + u(x)\underline{\boldsymbol{e}}_2, \quad \underline{\boldsymbol{\theta}} = \theta(x)\underline{\boldsymbol{e}}_3 \tag{14.10}$$

where the mean shear amount $\bar{\gamma}$ is prescribed to the strip. The total deformation and curvature tensors follow

$$\underset{\sim}{\boldsymbol{e}} = (\bar{\gamma} + \theta)\underline{\boldsymbol{e}}_1 \otimes \underline{\boldsymbol{e}}_2 + (u' - \theta)\underline{\boldsymbol{e}}_2 \otimes e_1, \quad \underset{\sim}{\boldsymbol{\kappa}} = \theta' \underline{\boldsymbol{e}}_3 \otimes \underline{\boldsymbol{e}}_1 \tag{14.11}$$

where $u(x)$ and $\theta(x)$ are the main unknowns of the problem. The notation u' is set for the derivative of $u(x)$ with respect to x.

The following boundary conditions are enforced:

$$u(0) = 0, \quad u(-L) = u(L), \quad \theta(-L) = \theta(L) = 0 \tag{14.12}$$

The first condition sets the rigid body translation and the second conditions correspond to periodicity requirement of the fluctuation $u(x)$. The micro-clamping conditions for the Cosserat rotation mimic the piling-up of dislocations at the left and boundaries.

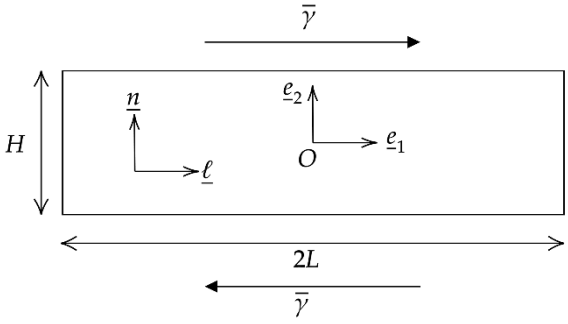

Fig. 14.1 Geometry of the simple shear boundary value problem in crystal plasticity involving a single slip system.

14.3 Cosserat Elastoplasticity Based on a Quadratic Potential

In this section, the Helmholtz free energy potential is assumed to be a quadratic function of the deformation measures

$$\psi(\underset{\sim}{\boldsymbol{e}}^e, \underset{\sim}{\boldsymbol{\kappa}}) = \frac{1}{2}\underset{\sim}{\boldsymbol{e}}^e : \underset{\sim}{\boldsymbol{\Lambda}} : \underset{\sim}{\boldsymbol{e}}^e + \frac{1}{2}\underset{\sim}{\boldsymbol{\kappa}} : \underset{\sim}{\boldsymbol{C}} : \underset{\sim}{\boldsymbol{\kappa}} \tag{14.13}$$

where $\underset{\sim}{\boldsymbol{\Lambda}}$ and $\underset{\sim}{\boldsymbol{C}}$ are the fourth order tensors of Cosserat elastic moduli. Point symmetry was assumed, thus excluding coupling terms between elastic deformation and curvature. The Cosserat elastic laws follow from Eq. (14.7)

$$\underset{\sim}{\boldsymbol{\sigma}} = \underset{\sim}{\boldsymbol{\Lambda}} : \underset{\sim}{\boldsymbol{e}}^e, \quad \underset{\sim}{\boldsymbol{m}} = \underset{\sim}{\boldsymbol{C}} : \underset{\sim}{\boldsymbol{\kappa}} \tag{14.14}$$

14.3.1 Simple Glide in Isotropic Elasticity

The boundary value problem of Sect. 14.2.3 is first solved in the case of linear isotropic elasticity, i.e. in the absence of plasticity. The isotropic elasticity laws read

$$\underset{\sim}{\boldsymbol{\sigma}} = \lambda \mathrm{trace}\,(\underset{\sim}{\boldsymbol{e}})\underset{\sim}{\boldsymbol{1}} + 2\mu \mathrm{sym}(\underset{\sim}{\boldsymbol{e}}) + 2\mu_c \mathrm{skew}(\underset{\sim}{\boldsymbol{e}}), \tag{14.15}$$

$$\underset{\sim}{\boldsymbol{m}} = \alpha \mathrm{trace}\,(\underset{\sim}{\boldsymbol{\kappa}})\underset{\sim}{\boldsymbol{1}} + 2\beta \mathrm{sym}(\underset{\sim}{\boldsymbol{\kappa}}) + 2\beta_2 \mathrm{skew}(\underset{\sim}{\boldsymbol{\kappa}}) \tag{14.16}$$

where $\lambda, \mu, \mu_c, \alpha, \beta, \beta_2$ are the six Cosserat elastic moduli required in the isotropic case. In the examples given in the present work, the parameter α is not active and we will assume $\beta_2 = \beta$ for simplicity [22].
In the particular case of simple shear, the non-vanishing components of the stress tensors are

$$\sigma_{12} = (\mu + \mu_c)\bar{\gamma} + (\mu - \mu_c)u' + 2\mu_c\theta, \tag{14.17}$$

$$\sigma_{21} = (\mu - \mu_c)\bar{\gamma} + (\mu + \mu_c)u' - 2\mu_c\theta, \tag{14.18}$$

$$m_{31} = 2\beta\theta' \tag{14.19}$$

The force stress balance tells that $\sigma_{12,2} = \sigma_{21,1} = 0$ so that σ_{21} is uniform. This provides a first differential equation

$$(\mu + \mu_c)u'' - 2\mu_c\theta' = 0 \quad \Longrightarrow \quad u'' = \frac{2\mu_c}{\mu + \mu_c}\theta' \tag{14.20}$$

On the other hand, the couple stress balance equation yields

$$m_{31,1} - (\sigma_{12} - \sigma_{21}) = 0 \tag{14.21}$$

$$\beta\theta'' - \mu_c(\bar{\gamma} - u' + 2\theta) = 0 \tag{14.22}$$

The combination of the previous equations leads to the following differential equation for θ

$$\theta''' = \omega^2 \theta', \quad \text{with} \quad \omega = \sqrt{\frac{2\mu\mu_c}{\beta(\mu+\mu_c)}} \tag{14.23}$$

from which the microrotation function is deduced, after consideration of the boundary conditions $(14.12)_3$,

$$\theta(x) = a(\cosh(\omega x) - \cosh(\omega L)) \tag{14.24}$$

The displacement function then follows from Eq. (14.20):

$$u(x) = \frac{2\mu_c}{\mu+\mu_c}\frac{a}{\omega}\sinh(\omega x) + bx + c \tag{14.25}$$

The boundary conditions $(14.12)_{1,2}$ are used to determine the constants b and c:

$$u(x) = \frac{2\mu_c}{\mu+\mu_c}\frac{a}{\omega}(\sinh(\omega x) - \frac{x}{L}\sinh(\omega L)) \tag{14.26}$$

The integration constant a is finally determined by inserting the found functions in Eq. (14.22):

$$a = \frac{\bar{\gamma}}{2(\cosh(\omega L) - \frac{\mu_c}{\mu+\mu_c}\frac{\sinh(\omega L)}{\omega L})} \tag{14.27}$$

Numerical simulations are carried out using the finite element code Z-Set [23]. More details regarding the implementation of the Cosserat element are given in reference [6]. The parameters given in Table 14.1 are used throughout this work, unless explicitly specified otherwise. Comparisons of the analytical and FEM solutions for the displacement and microrotation fields are plotted in Fig. 14.2, which shows a perfect agreement between the solutions.

Table 14.1: Parameters used for computing analytical and numerical solutions.

Parameter	value
2L [mm]	20
H [mm]	1
E [MPa]	70000
ν	0.3
μ_c [MPa]	10000
α [N]	0
β [N]	26923.8

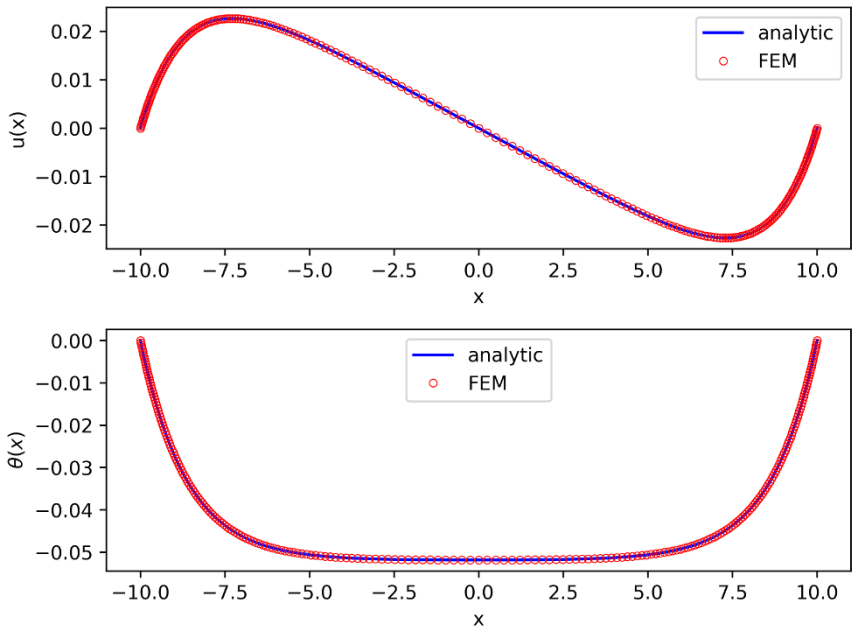

Fig. 14.2: Cosserat elasticity, displacement and microrotation fields. Finite Element simulations are compared to the analytical solution, based on the material parameters of Table 14.1.

14.3.2 Crystal Plasticity Based on the Full Stress Tensor

The resolved shear stress is computed as

$$\tau = \underset{\sim}{\boldsymbol{\sigma}} : (\underline{\boldsymbol{\ell}} \otimes \underline{\boldsymbol{n}}) = \underset{\sim}{\boldsymbol{\sigma}} : (\underline{\boldsymbol{e}}_1 \otimes \underline{\boldsymbol{e}}_2) = \sigma_{12} \tag{14.28}$$

In the plastic regime, assuming positive shear, $\tau = \tau_c$, the critical resolved shear stress is taken as a constant parameter (no hardening). Assuming that this plasticity threshold is reached in the whole specimen, the stress components σ_{12} and σ_{21} are therefore uniform during further straining. Space derivation of Eq. (14.21) implies that

$$m'_{31} = 0 \quad \Longrightarrow \quad \theta''' = 0 \tag{14.29}$$

It follows that the microrotation distribution in the strip is parabolic:

$$\theta(x) = a(x^2 - L^2) \tag{14.30}$$

with the integration constant a. The plastic and elastic deformation tensors take the form

$$\underset{\sim}{\boldsymbol{e}}^p = \gamma \, \underline{\boldsymbol{\ell}} \otimes \underline{\boldsymbol{n}} = \gamma \, \underline{\boldsymbol{e}}_1 \otimes \underline{\boldsymbol{e}}_2 \tag{14.31}$$

$$\underset{\sim}{\boldsymbol{e}}^e = \underset{\sim}{\boldsymbol{e}} - \underset{\sim}{\boldsymbol{e}}^p = (\bar{\gamma} + \theta - \gamma)\underline{\boldsymbol{e}}_1 \otimes \underline{\boldsymbol{e}}_2 + (u' - \theta)\underline{\boldsymbol{e}}_2 \otimes \underline{\boldsymbol{e}}_1 \tag{14.32}$$

where $\gamma(x)$ is the plastic slip distribution to be determined. In the presence of plasticity, the equations (14.17) and (14.18) are replaced by

$$\sigma_{12} = (\mu + \mu_c)(\bar{\gamma} - \gamma) + (\mu - \mu_c)u' + 2\mu_c\theta = \tau_c, \tag{14.33}$$

$$\sigma_{21} = (\mu - \mu_c)(\bar{\gamma} - \gamma) + (\mu + \mu_c)u' - 2\mu_c\theta \tag{14.34}$$

Elimination of γ in the previous equation and recalling that $\sigma'_{21} = 0$ due to equilibrium, leads to the following relation

$$u'' = \theta' \quad \Longrightarrow \quad u(x) = a\frac{x}{3}(x^2 - L^2) \tag{14.35}$$

where the displacement boundary conditions have been taken into account. The slip distribution is obtained from (14.33) and the found expressions for microrotation and displacement:

$$\gamma(x) = \bar{\gamma} - \frac{\tau_c}{\mu + \mu_c} + a\left(x^2 - \frac{\mu + 5\mu_c}{\mu + \mu_c}\frac{L^2}{3}\right) \tag{14.36}$$

The coefficient a is determined after insertion of $u(x)$ and $\theta(x)$ in the moment of momentum equation Eq. (14.21) which can be worked out as

$$(\mu + \mu_c)\beta\theta'' - \tau_c\mu_c + 2\mu\mu_c(u' - \theta) = 0 \tag{14.37}$$

Finally

$$a = \frac{\tau_c}{2\beta(1 + \mu/\mu_c) + 4\mu L^2/3} = \frac{\tau_c/2\mu}{\beta(1/\mu + 1/\mu_c) + 2L^2/3} \tag{14.38}$$

To highlight the size effect induced by the Cosserat model, the stress component σ_{21} is computed as a function of the parameter β and structural length L:

$$\sigma_{21} = \frac{\mu - \mu_c}{\mu + \mu_c}\tau_c + \frac{4\mu\mu_c}{\mu + \mu_c}(u' - \theta) \tag{14.39}$$

$$= \frac{\mu - \mu_c}{\mu + \mu_c}\tau_c + \frac{8}{3}\frac{\mu\mu_c}{\mu + \mu_c}aL^2 \tag{14.40}$$

$$= \tau_c\left(\frac{\mu - \mu_c}{\mu + \mu_c} + \frac{4\mu\mu_c}{\mu + \mu_c}\frac{L^2}{3\beta(1 + \mu/\mu_c) + 2\mu L^2}\right) \tag{14.41}$$

The limit case $\mu_c \to \infty$ can be more easily interpreted:

$$\lim_{\mu_c \to \infty} \sigma_{21}/\tau_c = -1 + \frac{4\mu L^2}{3\beta + 2\mu L^2} = \tau_c\frac{1 - 3\beta/2\mu L^2}{1 + 3\beta/2\mu L^2} \tag{14.42}$$

Where $\beta \to 0$, the classical limit $\sigma_{21} = \sigma_{12} = \tau_c$ with a symmetric stress tensor, is retrieved. For vanishing system size $L \to 0$, $\sigma_{21} = -\sigma_{12} = -\tau_c$ and the stress tensor is skew-symmetric.

14.3.3 Schmid Law Limited to the Symmetric Part of the Stress Tensor

A variant of the previous analysis is the consideration of a modification of the generalized Schmid law (14.8):

$$f(\underset{\sim}{\boldsymbol{\sigma}}, \underline{\boldsymbol{\ell}}, \underline{\boldsymbol{n}}) = |\tau| - \tau_c, \quad \text{with} \quad \mathrm{sym}(\underset{\sim}{\boldsymbol{\sigma}}) : (\underline{\boldsymbol{\ell}} \otimes \underline{\boldsymbol{n}}) \tag{14.43}$$

According to this variant, the resolved shear stress is computed from the projection of the symmetric part of the stress tensor instead of the full stress tensor.

The analysis of the one-dimensional shear layer problem is modified as follows.

$$\tau = (\sigma_{12} + \sigma_{21})/2 = \tau_c \tag{14.44}$$

assuming positive shear loading. This yield condition combined with balance of momentum implies that both σ_{12} and σ_{21} are uniform as in the previous section. It follows that the microrotation profile (14.30) is unchanged in the analysis. This holds true for Eqs. (14.31) and (14.32).

A difference arises in the evaluation of the resolved shear stress

$$\sigma_{12} + \sigma_{21} = 2\mu(\bar{\gamma} - \gamma) + 2\mu u' = 2\tau_c \tag{14.45}$$

but the same relation $u'' = \theta'$ is finally obtained, implying the same displacement profile (14.35). The constant a is determined from Eq. (14.37) which is modified here as

$$\beta\theta'' - \frac{\mu_c}{\mu}\tau_c + 2\mu_c(u' - \theta) = 0 \tag{14.46}$$

and finally

$$a = \frac{\tau_c/2\mu}{\beta/\mu_c + 2L^2/3} \tag{14.47}$$

$$\gamma(x) = \bar{\gamma} - \frac{\tau_c}{\mu} + a(x^2 - L^2/3) \tag{14.48}$$

which are slightly different from (14.38) and (14.36).

The stress components are then computed as

$$\sigma_{12} = \tau_c\left(1 + \frac{\mu_c}{\mu}\right) - \frac{4}{3}\mu_c a L^2 \tag{14.49}$$

$$\sigma_{21} = \tau_c\left(1 - \frac{\mu_c}{\mu}\right) + \frac{4}{3}\mu_c a L^2 \tag{14.50}$$

The first equation yields the following scaling with the size L of the system

$$\sigma_{12}/\tau_c = 1 + \frac{\beta/\mu}{\beta/\mu_c + 2L^2/3} \tag{14.51}$$

In the limit case,

$$\lim_{\mu_c \to \infty} \sigma_{12}/\tau_c = 1 + \frac{3\beta}{2\mu L^2} \tag{14.52}$$

making the $1/L^2$ scaling clearly visible. This scaling is rather questionable according to physical metallurgy which rather predicts $1/L$ (Orowan) or $1/\sqrt{L}$ (Hall-Petch) scaling laws in plasticity [13, 24].

14.3.4 Comparison with the $\mathbf{Curl}\, H^p$ *Model*

According to the theory developed in [15], the displacement gradient is split into elastic and plastic contributions:

$$\underset{\sim}{\boldsymbol{H}} = \mathrm{grad}\, \underline{\boldsymbol{u}} = \underset{\sim}{\boldsymbol{H}}^e + \underset{\sim}{\boldsymbol{H}}^p \tag{14.53}$$

The free energy density of the $\mathrm{Curl}\, H^p$ model is taken as a quadratic form

$$\psi(\underset{\sim}{\boldsymbol{\varepsilon}}^e, \mathrm{curl}\, \underset{\sim}{\boldsymbol{H}}^p) = \frac{1}{2} \underset{\sim}{\boldsymbol{\varepsilon}}^e : \underset{\approx}{\boldsymbol{\Lambda}} : \underset{\sim}{\boldsymbol{\varepsilon}}^e + A \| \mathrm{curl}\, \underset{\sim}{\boldsymbol{H}}^p \|^2 \tag{14.54}$$

where the elastic strain $\underset{\sim}{\boldsymbol{\varepsilon}}^e$ is the symmetric part of $\underset{\sim}{\boldsymbol{H}}^e$ and A the higher order modulus. The $\mathrm{curl}\, H^p$ model involves a size-dependent back-stress

$$x = -A(\mathrm{curl}\, \mathrm{curl}\, H^p) : (\underline{\boldsymbol{\ell}} \otimes \underline{\boldsymbol{n}}) \tag{14.55}$$

The Schmid law is generalized into

$$f(\underset{\sim}{\boldsymbol{\sigma}}, x, \underline{\boldsymbol{\ell}}, \underline{\boldsymbol{n}}) = |\tau - x| - \tau_c \tag{14.56}$$

and

$$\underset{\sim}{\dot{\boldsymbol{H}}}^p = \dot{\gamma}\, \underline{\boldsymbol{\ell}} \otimes \underline{\boldsymbol{n}}\, \mathrm{sign}\,(\tau - x) \quad \text{with} \quad \tau = \underset{\sim}{\boldsymbol{\sigma}} : (\underline{\boldsymbol{\ell}} \otimes \underline{\boldsymbol{n}}) \tag{14.57}$$

When applied to the studied boundary value problem, the $\mathrm{Curl}\, H^p$ model predicts the following:

$$\underset{\sim}{\boldsymbol{H}} = \bar{\gamma}\, \underline{\boldsymbol{e}}_1 \otimes \underline{\boldsymbol{e}}_2 + u' \underline{\boldsymbol{e}}_2 \otimes \underline{\boldsymbol{e}}_1, \quad \underset{\sim}{\boldsymbol{H}}^p = \gamma\, \underline{\boldsymbol{e}}_1 \otimes \underline{\boldsymbol{e}}_2 \tag{14.58}$$

$$\mathrm{curl}\, \underset{\sim}{\boldsymbol{H}}^p = -\gamma'\, \underline{\boldsymbol{e}}_1 \otimes \underline{\boldsymbol{e}}_3, \quad \mathrm{curl}\, \mathrm{curl}\, H^p = -\gamma''\, \underline{\boldsymbol{e}}_1 \otimes \underline{\boldsymbol{e}}_2, \quad x = -A\gamma'' \tag{14.59}$$

The single non-vanishing component of the stress tensor is

$$\sigma_{12} = \sigma_{21} = \mu(\bar{\gamma} - \gamma + u') \tag{14.60}$$

The Schmid law then stipulates that

$$\sigma_{12} + A\gamma'' = \tau_c \tag{14.61}$$

Equilibrium $\sigma_{21,1} = 0$ requires that the shear stress is uniform. The previous equations then implies that $\gamma''' = 0$ so that the slip distribution is parabolic as in the Cosserat case. Boundary conditions must be chosen to represent the fact that no plasticity occurs at the boundaries:

$$\gamma(\pm L) = 0 \quad \Longrightarrow \quad \gamma(x) = a(L^2 - x_2) \tag{14.62}$$

Note that these conditions are only approximately equivalent to those chosen for the Cosserat medium, namely vanishing lattice rotation $\theta(\pm L) = 0$.

The stress is then related to coefficient a by

$$\sigma_{12} = \tau_c - Aa \tag{14.63}$$

The displacement is derived from Eq. (14.60):

$$\begin{aligned} u' &= \frac{\sigma_{12}}{\mu} - \bar{\gamma} + \gamma \\ u &= (\frac{\tau_c - Aa}{\mu} - \bar{\gamma} + aL^2)x - a\frac{x^3}{3} + Cste \end{aligned} \tag{14.64}$$

The constant vanishes since $u(0) = 0$. The condition $u(-L) = u(L)$ is used to determine the remaining constant a:

$$a = \frac{3}{2L^2}\left(\frac{\tau_c}{\mu} - \bar{\gamma}\right) \tag{14.65}$$

and finally, the shear stress value

$$\sigma_{12} = \tau_c - \frac{3A}{2L^2}\left(\frac{\tau_c}{\mu} - \bar{\gamma}\right) \tag{14.66}$$

The $1/L^2$ scaling is clearly observed and is in agreement with the Cosserat solutions [16]. Quadratic potentials in Cosserat or strain gradient plasticity therefore suffer from the same limitations compared to common knowledge in mechanical metallurgy.

14.4 Rank One Energy Potential

In this section, a non-quadratic free energy potential is adopted

$$\psi(\underset{\sim}{\boldsymbol{e}}^e, \underset{\sim}{\boldsymbol{\kappa}}) = \frac{1}{2}\underset{\sim}{\boldsymbol{e}}^e : \underset{\approx}{\boldsymbol{\Lambda}} : \underset{\sim}{\boldsymbol{e}}^e + A\|\underset{\sim}{\boldsymbol{\kappa}}\|, \quad \text{with} \quad \|\underset{\sim}{\boldsymbol{\kappa}}\| = \sqrt{\underset{\sim}{\boldsymbol{\kappa}} : \underset{\sim}{\boldsymbol{\kappa}}} \tag{14.67}$$

involving the norm of the curvature tensor. The simple and couple stress tensors are then given by

$$\underset{\sim}{\boldsymbol{\sigma}} = \frac{\partial \psi}{\partial \underset{\sim}{\boldsymbol{e}}^e} = \underset{\approx}{\boldsymbol{\Lambda}} : \underset{\sim}{\boldsymbol{e}}^e \tag{14.68}$$

$$\underset{\sim}{\boldsymbol{m}} = \frac{\partial \psi}{\partial \underset{\sim}{\boldsymbol{\kappa}}} = A \frac{\underset{\sim}{\boldsymbol{\kappa}}}{\|\underset{\sim}{\boldsymbol{\kappa}}\|} \tag{14.69}$$

It is apparent that the couple stress tensor is singular in the case of vanishing curvature.

In the one-dimensional shear problem studied here, the single non-vanishing component of the couple stress tensor is

$$m_{31} = A \frac{\theta'}{|\theta'|} \tag{14.70}$$

14.4.1 Elasticity Solution

In the elastic case, $\underset{\sim}{\boldsymbol{e}}^e \equiv \underset{\sim}{\boldsymbol{e}}$. The microrotation profile is searched for in the following form:

$$\theta(x) = \bar{\theta}(H(x+L) - H(x-L)) \tag{14.71}$$

$$\theta'(x) = \bar{\theta}(\delta(x+L) - \delta(x-L)) \tag{14.72}$$

which means that the microrotation takes the unknown uniform value $\bar{\theta}$ in $]-L:L]$ and is indeterminate at the ends of the interval. The expression involves the Heaviside function and the Dirac distribution such that

$$H'(x-a) = \delta(x-a) \tag{14.73}$$

The uniform rotation field corresponds to the classical solution in the absence of curvature. The difference in the Cosserat case is that curvature energy is now concentrated at the boundaries.

It follows that the couple stress component is indeterminate due to the vanishing of θ'. The total work balance equation is therefore used for a suitable treatment of the distribution functions:

$$\int_V \underset{\sim}{\boldsymbol{\sigma}} : (\underline{\boldsymbol{u}} \otimes \boldsymbol{\nabla} + \underset{\approx}{\boldsymbol{\epsilon}} \cdot \underline{\boldsymbol{\theta}}) + \underset{\sim}{\boldsymbol{m}} : \underset{\sim}{\boldsymbol{\kappa}}\, dV = \int_{\partial V} \underline{\boldsymbol{t}} \cdot \underline{\boldsymbol{u}} + \underline{\boldsymbol{m}} \cdot \underline{\boldsymbol{\theta}}\, dS \tag{14.74}$$

The volume V is the infinite ribbon $[-L:L] \times \mathbb{R}$ and invariance along y is assumed. The application of the divergence theorem and the Neumann condition $\underline{\boldsymbol{t}} = \underset{\sim}{\boldsymbol{\sigma}} \cdot \underline{\boldsymbol{n}}$ are used to eliminate the $\underline{\boldsymbol{u}} \otimes \boldsymbol{\nabla}$ and $\underline{\boldsymbol{t}} \cdot \underline{\boldsymbol{u}}$ terms Eq. (14.74), while the last term vanishes due to the vanishing microrotation boundary conditions. It remains

$$\int_V \underset{\sim}{\boldsymbol{\sigma}} : \underset{\approx}{\boldsymbol{\epsilon}} \cdot \underline{\boldsymbol{\theta}} + \underset{\sim}{\boldsymbol{m}} : (\underline{\boldsymbol{\theta}} \otimes \boldsymbol{\nabla})\, dV = 0 \tag{14.75}$$

Keeping only the non-vanishing components, the latter becomes

$$\int_{-L}^{L}(\sigma_{12}-\sigma_{21})\theta+m_{31}\theta'\,dx=\int_{-L}^{L}(\sigma_{12}-\sigma_{21})\theta+A|\theta'|\,dx=0 \tag{14.76}$$

where $m_{31}\theta'=A\theta'^2/|\theta'|$ has been used. After considering Eq. (14.72), the last integral is evaluated as

$$\int_{-L}^{L}A|\theta'|dx=A|\bar{\theta}|\int|(\delta(x+L)-\delta(x-L))|dx=2A|\bar{\theta}| \tag{14.77}$$

The first contribution in Eq. (14.76) is then evaluated as

$$\int_{-L}^{L}(\sigma_{12}-\sigma_{21})\theta\,ds=\int_{-L}^{L}2\mu_c(\bar{\gamma}-u'+2\theta)\theta\,ds=4\mu_c\bar{\theta}L(\bar{\gamma}+2\bar{\theta}) \tag{14.78}$$

taking the periodicity of u into account. Finally, the combination of the two found relations provides the value

$$\bar{\theta}=-\frac{\bar{\gamma}}{2}-\frac{A}{4\mu_c L}\text{sign}\bar{\theta}=-\frac{\bar{\gamma}}{2}+\frac{A}{4\mu_c L}\text{sign}\bar{\gamma} \tag{14.79}$$

where $\bar{\theta}$ and $\bar{\gamma}$ have opposite signs for sufficiently high values of μ_c. The limit case $\mu_c\to+\infty$ constrains $\bar{\theta}$ to coincide with the material rotation $-\bar{\gamma}/2$.

Finally, the displacement field is obtained from the shear stress component

$$\sigma_{21}=(\mu+\mu_c)u'+(\mu-\mu_c)\bar{\gamma}-2\mu_c\theta \tag{14.80}$$

According to equilibrium, this component is uniform from which we deduce that $u''=0$ so that $u(x)$ is linear.

The couple stress component m_{31} is indeterminate in the interval $]-L:L[$ where θ' vanishes. Let us assume that it is uniform in this interval. This, combined with the balance of moment of momentum equation, implies that the skew symmetric part of the stress tensor also vanishes. Finally,

$$u=(\bar{\gamma}+2\theta)x=\frac{A}{2\mu_c L}x\,\text{sign}\,\bar{\gamma},\quad\forall x\in]-L:L[\tag{14.81}$$

This fluctuation vanishes for $\mu_c\to\infty$ or vanishing length scale.

14.4.2 Crystal Plasticity

In the crystal plasticity case, the shear stress component σ_{12} is equal to the critical resolved shear stress value. Eq. (14.76) is still valid and now provides the relation

$$(\tau_c-\sigma_{21})\bar{\theta}2L+2A|\bar{\theta}|=0 \tag{14.82}$$

Equilibrium still implies that σ_{21} is uniform. Its value follows

$$\sigma_{21} = \tau_c + \frac{A}{L}\text{sign}\bar{\theta} \tag{14.83}$$

The scaling in $1/L$ is clearly visible and is distinct from the $1/L^2$ scaling law found for the quadratic potential.

On the other hand, the elasticity law tells us that

$$\sigma_{12} - \sigma_{21} = 2\mu_c(\bar{\gamma} - \gamma(x) - u'(x)) + 4\mu_c\theta \tag{14.84}$$

Averaging this relation over the interval $[-L : L]$ and assuming periodicity of displacement give

$$\tau_c - \sigma_{21} = 2\mu_c < \bar{\gamma} - \gamma > +4\mu_c\bar{\theta} \tag{14.85}$$

The average $< \bar{\gamma} - \gamma >$ is deduced from Eq. (14.33) as

$$< \bar{\gamma} - \gamma >= (\tau_c - 2\mu_c\bar{\theta})/(\mu + \mu_c) \tag{14.86}$$

and finally

$$\frac{2\mu_c}{\mu + \mu_c}(\tau_c + 2\mu\bar{\theta}) = -\frac{A}{L}\text{sign}\bar{\theta} \tag{14.87}$$

from which the constant $\bar{\theta}$ is derived:

$$\bar{\theta} = -\frac{\tau_c}{2\mu} - \frac{A}{L}\frac{\mu + \mu_c}{4\mu\mu_c}\text{sign}\bar{\theta} \tag{14.88}$$

14.4.3 Comparison with the $\mathbf{Curl}\,H^p$ *Model*

A rank one potential was also considered in [15, 25]:

$$\psi(\underset{\sim}{\boldsymbol{\varepsilon}}^e, \text{curl}\,\underset{\sim}{\boldsymbol{H}}^p) = \frac{1}{2}\underset{\sim}{\boldsymbol{\varepsilon}}^e : \underset{\approx}{\boldsymbol{\Lambda}} : \underset{\sim}{\boldsymbol{\varepsilon}}^e + A\|\text{curl}\,\underset{\sim}{\boldsymbol{H}}^p\| \tag{14.89}$$

involving the norm of the dislocation density $\mathbf{curl}\,H^p$. The symmetric stress tensor and the higher order stress are then computed as

$$\underset{\sim}{\boldsymbol{\sigma}} = \underset{\approx}{\boldsymbol{\Lambda}} : \underset{\sim}{\boldsymbol{\varepsilon}}^e, \quad \underset{\sim}{\boldsymbol{m}} = A\frac{\text{curl}\,\underset{\sim}{\boldsymbol{H}}^p}{\|\text{curl}\,\underset{\sim}{\boldsymbol{H}}^p\|} \tag{14.90}$$

In the studied problem,

$$\text{curl}\,\underset{\sim}{\boldsymbol{H}}^p = -\gamma'\,\underline{\boldsymbol{e}}_1 \otimes \underline{\boldsymbol{e}}_3, \quad \underset{\sim}{\boldsymbol{m}} = -A\text{sign}\,\gamma' \tag{14.91}$$

It was shown in [15, 25] that the total work balance reduces to the integral

$$\int_V \underset{\sim}{\boldsymbol{s}} : \underset{\sim}{\boldsymbol{H}}^p + \underset{\sim}{\boldsymbol{m}} : \text{curl}\,H^p\,dV = 0 \tag{14.92}$$

where the involved generalized stress tensors fulfil the balance law, $\underset{\sim}{\boldsymbol{s}} + \operatorname{curl} \underset{\sim}{\boldsymbol{m}} = 0$. For the studied problem, this amounts to

$$\int_{-L}^{L} s_{12}\gamma + A|\gamma'|\, dx = 0 \tag{14.93}$$

According to the Schmid law,

$$\sigma_{12} + s_{12} = \tau_c \tag{14.94}$$

where both σ_{12} and s_{12} are uniform.
The plastic slip distribution is uniform in $]-L : L[$:

$$\gamma(x) = \bar{\gamma}(H(x+L) - H(x-L)) \tag{14.95}$$

$$\gamma'(x) = \bar{\gamma}(\delta(x+L) - \delta(x-L)) \tag{14.96}$$

Finally, the previous integral is calculated as

$$(\tau_c - \sigma_{12})2L\bar{\gamma} + 2A\bar{\gamma} = 0 \tag{14.97}$$

so that the stress value

$$\sigma_{12} = \tau_c + \frac{A}{L} \tag{14.98}$$

exhibits a $1/L$ size dependence, in the same way as the previous Cosserat model.

14.5 Combined Potential

In this section, a free energy involving both quadratic and norm potentials is considered

$$\psi(\underset{\sim}{\boldsymbol{e}}^e, \underset{\sim}{\boldsymbol{\kappa}}) = \frac{1}{2}\underset{\sim}{\boldsymbol{e}}^e : \underset{\approx}{\boldsymbol{\Lambda}} : \underset{\sim}{\boldsymbol{e}}^e + \frac{1}{2}\underset{\sim}{\boldsymbol{\kappa}} : \underset{\approx}{\boldsymbol{C}} : \underset{\sim}{\boldsymbol{\kappa}} + A\|\underset{\sim}{\boldsymbol{\kappa}}\|, \quad \text{with} \quad \|\underset{\sim}{\boldsymbol{\kappa}}\| = \sqrt{\underset{\sim}{\boldsymbol{\kappa}} : \underset{\sim}{\boldsymbol{\kappa}}} \tag{14.99}$$

The simple and couple stress tensors are then given by

$$\underset{\sim}{\boldsymbol{\sigma}} = \frac{\partial \psi}{\partial e^e} = \underset{\approx}{\boldsymbol{\Lambda}} : \underset{\sim}{\boldsymbol{e}}^e \tag{14.100}$$

$$\underset{\sim}{\boldsymbol{m}} = \frac{\partial \psi}{\partial \underset{\sim}{\boldsymbol{\kappa}}} = \underset{\approx}{\boldsymbol{C}} : \underset{\sim}{\boldsymbol{\kappa}} + A\frac{\underset{\sim}{\boldsymbol{\kappa}}}{\|\underset{\sim}{\boldsymbol{\kappa}}\|} \tag{14.101}$$

In the problem considered in this work, the only non-vanishing component of the couple-stress tensor is

$$m_{31} = 2\beta\theta' + A\frac{\theta'}{|\theta'|} \tag{14.102}$$

More precisely,

$$m_{31}(x) = 2\beta\theta - A, \quad \text{if} \quad x < 0 \tag{14.103}$$

$$m_{31}(x) = 2\beta\theta + A, \quad \text{if} \quad x > 0 \tag{14.104}$$

considering the situation where $\theta(x)$ is decreasing (resp. increasing) on $[-L, 0]$ (resp. $[0, L]$). In that case, the curvature is indeterminate only at $x = 0$. The field equations (14.21) to (14.23) from section 14.3.1 are valid in the present context. The solution has cosh form but there is a jump of sign θ' at zero. The micro-rotation field is therefore assumed to be of the following form:

$$\theta(x) = a^+ \cosh(\omega x) + b^+ \sinh(\omega x) + c^+, \quad \text{if} \quad x > 0 \tag{14.105}$$

$$= a^- \cosh(\omega x) + b^- \sinh(\omega x) + c^-, \quad \text{if} \quad x < 0 \tag{14.106}$$

The microtation field is an even function, $\theta(x) = \theta(-x)$, which results in

$$a^+ = a^- = a, \quad b^+ = -b^- = b, \quad c^+ = c^- \tag{14.107}$$

The boundary conditions, $\theta(-L) = \theta(L) = 0$, give

$$c = -(a\cosh(\omega L) + b\sinh(\omega L)) \tag{14.108}$$

The integration constant b can be found by ensuring the continuity of the couple stress at $x = 0$, $m_{31}(0^-) = m_{31}(0^+)$, due to the unhindered transmission of the couple stress vector,

$$2\beta\omega b + A = -2\beta\omega b - A \quad \Longrightarrow \quad b = \frac{-A}{2\beta\omega} \tag{14.109}$$

According to Eqs. (14.103) and (14.104), the continuity of m_{31} results in a jump of θ' at $x = 0$. Finally, the last integration constant a is obtained after integrating the equilibrium equation for the couple-stress

$$\int_{-L}^{L} m_{31,1} dx = \int_{-L}^{L} \sigma_{12} - \sigma_{21} dx \tag{14.110}$$

The couple stress $m_{31}(x)$ being an odd function, the left hand-side of the above equation is evaluated as

$$\int_{-L}^{L} m_{31,1} dx = 2 \lim_{\epsilon \to 0} \int_{\epsilon}^{L} m_{31,1}^{+} dx \tag{14.111}$$

$$\int_{-L}^{L} m_{31,1} dx = 4\beta\omega \left(a\sinh(\omega L) + b\cosh(\omega L)\right) + 2A \tag{14.112}$$

whereas the second integral to be evaluated gives

$$\int_{-L}^{L} \sigma_{12} - \sigma_{21} dx = \int_{-L}^{L} 2\mu_c \left(\bar{\gamma} - u' + 2\theta\right) dx \tag{14.113}$$

$$\int_{-L}^{L} \sigma_{12} - \sigma_{21} dx = 4\mu_c \left[\bar{\gamma} L + 2\left(\frac{a}{\omega}\sinh(\omega L) + \frac{b}{\omega}\left(\cosh(\omega L) - 1\right) + cL\right)\right] \tag{14.114}$$

where the periodicity of u and θ has been accounted for. Eq. (14.110) now becomes

$$\begin{aligned} &4\beta\omega\left(a\sinh(\omega L)+b\cosh(\omega L)\right)+2A \\ &\quad=4\mu_c\left[\bar{\gamma}L+2\left(\frac{a}{\omega}\sinh(\omega L)+\frac{b}{\omega}\left(\cosh(\omega L)-1\right)+cL\right)\right] \end{aligned} \tag{14.115}$$

After replacing the constants b and c by their found values one gets

$$a=\frac{2\mu\mu_c L\bar{\gamma}+A\left(L\omega(\mu+\mu_c)\sinh(\omega L)+\mu_c(1-\cosh(\omega L))\right)}{4\mu\mu_c L\cosh(\omega L)-2\mu_c\beta\omega\sinh(\omega L)} \tag{14.116}$$

The microrotation field is continuous at $x=0$ but its first derivative experiences a jump at this location.

14.6 Application to Grain Boundary Behaviour

The Cosserat model can be combined with a phase field approach to model grain boundary migration in polycrystals [26]. It originates from Kobayashi, Warren and Carter's model [17, 29] which relies on two phase field variables, the crystal orientation θ and the order parameter, called cristallinity parameter, ϕ. The KWC model is limited here to the 2D case, for which the orientation pseudo-vector reduces to the scalar θ and curvature vector $\boldsymbol{\nabla}\theta$, for the sake of brevity. After showing the connections between the KWC and Cosserat models, we report on an analytical solution for a sharp grain boundary and smooth order parameter profile, after [29, 30]. The KWC model is interpreted as a Cosserat-phase field model of grain boundaries [26].

14.6.1 Cosserat-Phase Field Model of Grain Boundaries

The Helmholtz free energy function of the KWC model is

$$\psi(\phi,\boldsymbol{\nabla}\phi,\boldsymbol{\nabla}\theta)=f(\phi)+\frac{\alpha^2}{2}\|\boldsymbol{\nabla}\phi\|^2+sg(\phi)\|\boldsymbol{\nabla}\theta\|+\frac{\varepsilon^2}{2}h(\phi)\|\boldsymbol{\nabla}\theta\|^2 \tag{14.117}$$

using the original notations of the authors. The potential (14.117) involves the two functions

$$f(\phi)=\frac{w^2}{2}(1-\phi)^2,\quad g(\phi)=h(\phi)=\phi^2 \tag{14.118}$$

and the material parameters w,α,s,ε^2. The situation $\phi=1$ corresponds to the perfect crystal whereas ϕ is minimal inside the grain boundary as a sign of disorder.

It is apparent that the potential combines a quadratic part for the curvature $\boldsymbol{\nabla}\theta$ and rank one part of the potential. The non-differentiability of the potential at $\boldsymbol{\nabla}\theta=0$ is

the source of mathematical difficulties, already seen in the Sect. 14.4 dedicated to the similar rank-one potential. A mathematical discussion can be found in [31].

The field equations can be derived from the method of virtual power by introducing the following power densities of generalized internal and contact forces:

$$p^{(i)} = a\dot{\phi} + \underline{\boldsymbol{b}} \cdot \boldsymbol{\nabla}\dot{\phi} + 2\overset{\times}{\sigma}\dot{\theta} + \underline{\boldsymbol{m}} \cdot \boldsymbol{\nabla}\dot{\theta} \tag{14.119}$$

$$p^{(c)} = a^c\dot{\phi} + m\dot{\theta} \tag{14.120}$$

The balance laws are derived in the form

$$a = \operatorname{div}\underline{\boldsymbol{b}}\,, \quad 2\overset{\times}{\sigma} = \operatorname{div}\underline{\boldsymbol{m}} \tag{14.121}$$

The second equation can be interpreted as part of the moment of momentum balance equation for a Cosserat medium, with $\underline{\boldsymbol{m}}$ having the physical dimension of couple stresses. They are complemented by the Neumann conditions

$$a^c = \underline{\boldsymbol{b}} \cdot \underline{\boldsymbol{n}}\,, \quad m = \underline{\boldsymbol{m}} \cdot \underline{\boldsymbol{n}} \tag{14.122}$$

The Clausius-Duhem inequality can be exploited to propose the following state laws:

$$\underline{\boldsymbol{b}} = \frac{\partial\psi}{\partial\boldsymbol{\nabla}\phi}, \quad \underline{\boldsymbol{m}} = \frac{\partial\psi}{\partial\boldsymbol{\nabla}\theta}, \quad a = \frac{\partial\psi}{\partial\phi} + a^{dis} \tag{14.123}$$

The introduction of the dissipative contribution a^{dis} was proposed by Fried and Gurtin [27, 28]. The residual dissipation rate then is

$$a^{dis}\dot{\phi} + 2\overset{\times}{\sigma}\dot{\theta} \geq 0 \tag{14.124}$$

The following dissipation potential is introduced

$$\Omega(a^{dis}, \overset{\times}{\sigma}) = \frac{1}{2M}(a^{dis})^2 + \frac{\overset{\times}{\sigma}^2}{\eta} \tag{14.125}$$

from which the evolution equations are derived

$$\dot{\phi} = \frac{\partial\Omega}{\partial a^{dis}} = a^{dis}/\beta = (a - \frac{\partial\psi}{\partial\phi})/\beta \tag{14.126}$$

$$\dot{\theta} = \frac{\partial\Omega}{\partial\overset{\times}{\sigma}} = 2\overset{\times}{\sigma}/\eta = (\operatorname{div}\underline{\boldsymbol{m}})/\eta = (\operatorname{div}\frac{\partial\psi}{\partial\boldsymbol{\nabla}\theta})/\eta \tag{14.127}$$

After substitution of the state laws derived from the free energy potential (14.117), the evolution equations are explicited as

$$\beta\dot{\phi} = \alpha^2\Delta\phi + w^2(1-\phi) - 2s\phi\|\boldsymbol{\nabla}\theta\| - \varepsilon^2\phi\|\theta\|^2 \tag{14.128}$$

$$2\eta = \operatorname{div}\left(s\phi^2\frac{\boldsymbol{\nabla}\theta}{\|\boldsymbol{\nabla}\theta\|} + \varepsilon^2\phi^2\boldsymbol{\nabla}\phi\right) \tag{14.129}$$

The fields $\phi = 1, \nabla\theta = 0$ are stationary solutions of the previous evolution equations. It corresponds to bulk crystal without lattice rotation and perfectly ordered crystal $\phi = 1$.

14.6.2 Analytical Solution of a Single Flat Grain Boundary

Analytical solutions of grain boundary formation with the KWC model is not an easy task. Such a solution can be worked out in the case $\varepsilon = 0$, assuming a sharp interface with respect to orientation and smooth with respect to the order parameter, see [29, 30]. The problem is 1D along x with an infinite flat grain boundary perpendicular to the -axis. The orientation is assumed to be piece-wise uniform with a jump at $x = 0$ in the 1D system. The orientation profile is taken of the form

$$[[\theta]] = \theta^+ - \theta^-, \quad \nabla\theta(x) = [[\theta]]\delta(x) \tag{14.130}$$

We then search for the order parameter field $\phi(x)$, solution of Eq. (14.128):

$$\alpha^2\phi'' + w^2(1-\phi) - 2s\phi|\theta'| = 0 \tag{14.131}$$

The second equation (14.129) becomes

$$\text{div}\left(s\phi^2\frac{\theta'}{|\theta'|}\right) = 0 \tag{14.132}$$

It is identically fulfilled almost everywhere.

For $x \neq 0$, Eq. (14.131) becomes

$$\alpha^2\phi'' + w^2(1-\phi) = 0 \tag{14.133}$$

which provides the solution

$$\phi(x) = C_1^+\exp(-wx/\alpha) + C_2^+\exp(wx/\alpha) + 1, \quad \forall x > 0 \tag{14.134}$$

$$\phi(x) = C_1^-\exp(-wx/\alpha) + C_2^-\exp(wx/\alpha) + 1, \quad \forall x < 0 \tag{14.135}$$

Full cristallinity is enforced at $x = \pm\infty$, $\phi(\pm\infty) = 1$ so that $C_2^+ = C_1^- = 0$. Continuity of ϕ is assumed at $x = 0$, $\phi(0^+) = \phi(0^-) = \phi_{min}$ so that $C_1^+ = C_2^-$ and finally

$$\phi(x) = 1 - C\exp(-w|x|/\alpha), \quad C = 1 - \phi_{min} \tag{14.136}$$

$$\phi'(x) = C\frac{w}{\alpha}\exp(-w|x|/\alpha)\text{sign}(x) \tag{14.137}$$

Determination of ϕ_{min}

For that purpose, the field equation (14.131) is integrated over the interval $[-\epsilon : \epsilon]$:

$$\int_{-\epsilon}^{\epsilon} \alpha^2 \phi'' dx + \int_{-\epsilon}^{\epsilon} w^2 (1-\phi) dx - 2s \int_{-\epsilon}^{\epsilon} \phi |\theta'| = 0 \tag{14.138}$$

Letting $\epsilon \to 0$, the second term vanishes due to continuity of the integrand and it remains

$$\alpha^2 [[\phi']] = 2s\phi(0)[[\theta]] \tag{14.139}$$

and finally

$$\alpha^2 (\phi'(0^+) - \phi'(0^-)) = 2\alpha^2 (1-\phi_{min}) \frac{w}{\alpha} = 2s\phi_{min}[[\theta]] \tag{14.140}$$

The last equation provides the value of ϕ_{min}:

$$\phi_{min} = \frac{w\alpha}{w\alpha + s[[\theta]]} = \left(1 + \frac{s}{w\alpha}[[\theta]]\right)^{-1} \tag{14.141}$$

This expression displays two limit cases: vanishing orientation jump gives $\phi_{min}([[\theta]] = 0) = 1$, as it should be, and

$$\lim_{[[\theta]] \to \infty} \phi_{min} = 0 \tag{14.142}$$

which means that lower values of the order parameter are reached for higher misorientation between the grains.

14.6.3 Grain Boundary Energy

The energy of the diffuse grain boundary is computed from the following integral of the energy density over the entire domain

$$\gamma_{GB} = \int_{-\infty}^{+\infty} \frac{w^2}{2}(1-\phi)^2 + \frac{\alpha^2}{2}\phi'^2 + s\phi^2 |\theta'| \, dx \tag{14.143}$$

The first two integrals are computed as follows

$$\begin{aligned} \int_{-\infty}^{+\infty} (1-\phi)^2 \, dx &= C^2 \int_{-\infty}^{+\infty} \exp(-\frac{2w}{\alpha}|x|) \, dx \\ &= \int_{-\infty}^{0} \exp(\frac{2w}{\alpha}x) \, dx + \int_{0}^{+\infty} \exp(-\frac{2w}{\alpha}x) \, dx \\ &= C^2 \frac{\alpha}{w} \end{aligned} \tag{14.144}$$

$$\int_{-\infty}^{+\infty} \phi'^2 \, dx = C^2 \frac{w}{\alpha} \tag{14.145}$$

Finally

$$\begin{aligned}\gamma_{GB} &= C^2\alpha w + s[[\theta]]\phi_{min}^2 \\ &= (1-\phi_{min})^2\alpha w + s[[\theta]]\phi_{min}^2 \\ &= \left(\frac{1}{s[[\theta]]} + \frac{1}{w\alpha}\right)^{-1}\end{aligned} \tag{14.146}$$

This energy vanishes when $[[\theta]]$, as expected. This formula and the choice of the diffuse interface width enable calibration of the parameters s, w, α. It is complemented by proper fitting to the Read-Shockley energy profile for low angle grain boundaries.

After proper non-dimensionalising of the model with respect to ω and introduction of time and length scales [29], the profiles of phase-fields ϕ and θ are given in Fig. 14.3 for arbitrarily chosen parameters $w = 1, \alpha = 0.3, s = 2$. A dimensionless grain boundary energy-misorientation curve is given in Fig. 14.4.

A calibration of the phase-field parameters can also be carried out. Whereas parameter ϵ is a choice allowing to change the interfaces width, parameters w, α, s are given by an optimisation procedure aiming to fit the grain boundary energy-misorientation curve of the model to the Read-Shockley part of the one given by real data. For more details on the calibration procedure the reader is referred to Appendix B of reference [26].

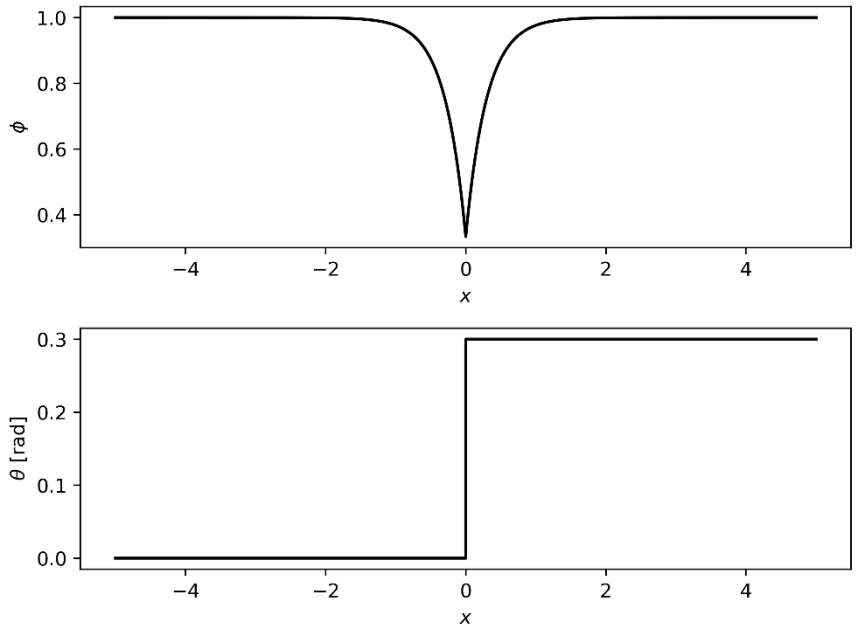

Fig. 14.3: Profiles of ϕ and θ in the sharp interface case.

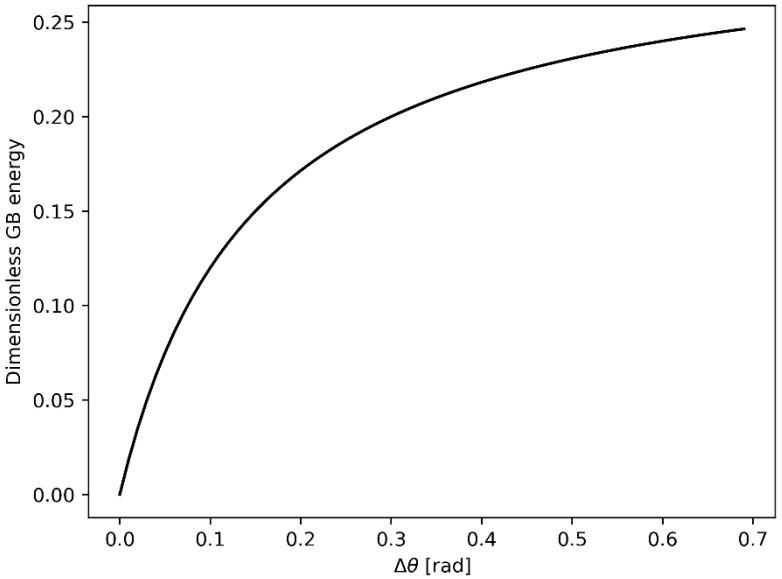

Fig. 14.4: Dimensionless grain boundary energy-misorientation curve.

References

[1] McClintock F, André P, Schwerdt K, Stoeckly R (1958) Interface couples in crystals, Nature **4636**:652–653.

[2] Kröner E (1963) On the physical reality of torque stresses in continuum mechanics, Int J Engng Sci **1**:261–278.

[3] Mayeur JR, McDowell DL, Forest S (2018) Micropolar crystal plasticity, In: GZ Voyiadjis (Ed) Handbook of Nonlocal Continuum Mechanics for Materials and Structures, pp 1–47, Springer International Publishing. DOI 10.1007/978-3-319-22977-5_48-1

[4] Forest S, Mayeur JR, McDowell DL (2018) Micromorphic crystal plasticity, In: GZ Voyiadjis (Ed) Handbook of Nonlocal Continuum Mechanics for Materials and Structures, pp 1–44, Springer International Publishing. DOI 10.1007/978-3-319-22977-5_49-1

[5] Forest S, Cailletaud G, Sievert R (1997) A Cosserat theory for elastoviscoplastic single crystals at finite deformation, Archives of Mechanics **49**(4):705–736.

[6] Forest S, Barbe F, Cailletaud G (2000) Cosserat modelling of size effects in the mechanical behaviour of polycrystals and multiphase materials, International Journal of Solids and Structures **37**:7105–7126.

[7] Mayeur J, McDowell D, Bammann D (2011) Dislocation–based micropolar single crystal plasticity: Comparison of multi– and single criterion theories, Journal of the Mechanics and Physics of Solids **59**:398–422.
[8] Mayeur J, McDowell D (2014) A comparison of Gurtin type and micropolar theories of generalized single crystal plasticity, International Journal of Plasticity **57**:29–51. DOI http://dx.doi.org/10.1016/j.ijplas.2014.01.010
[9] Rys M, Stupkiewicz S, Petryk H (2022) Micropolar regularization of crystal plasticity with the gradient-enhanced incremental hardening law, International Journal of Plasticity **156**:103355. DOI 10.1016/j.ijplas.2022.103355
[10] Gurtin M (2003) On a framework for small–deformation viscoplasticity: free energy, microforces, strain gradients, International Journal of Plasticity **19**:47–90.
[11] Gurtin M, Anand L (2009) Thermodynamics applied to gradient theories involving the accumulated plastic strain: The theories of Aifantis and Fleck & Hutchinson and their generalization, Journal of the Mechanics and Physics of Solids **57**:405–421.
[12] Ohno N, Okumura D (2007) Higher–order stress and grain size effects due to self–energy of geometrically necessary dislocations, Journal of the Mechanics and Physics of Solids **55**:1879–1898.
[13] Forest S (2013) Questioning size effects as predicted by strain gradient plasticity, Journal of the Mechanical Behavior of Materials **22**:101–110.
[14] Forest S, Guéninchault N (2013) Inspection of free energy functions in gradient crystal plasticity, Acta Mechanica Sinica **29**:763–772.
[15] Wulfinghoff S, Forest S, Böhlke T (2015) Strain gradient plasticity modeling of the cyclic behavior of laminate microstructures, Journal of the Mechanics and Physics of Solids **79**:1–20. DOI 10.1016/j.jmps.2015.02.008
[16] Cordero NM, Gaubert A, Forest S, Busso E, Gallerneau F, Kruch S (2010) Size effects in generalised continuum crystal plasticity for two–phase laminates, Journal of the Mechanics and Physics of Solids **58**:1963–1994.
[17] Kobayashi R, Warren JA, Carter WC (2000) A continuum model of grain boundaries, Physica D **140**(1-2):141–150.
[18] Nowacki W (1986) Theory of Asymmetric Elasticity, Pergamon.
[19] Eringen A (1999) Microcontinuum Field Theories, Springer, New York (1999)
[20] Ghiglione F, Forest S (2022) On the torsion of isotropic elastoplastic Cosserat circular cylinders, Journal of Micromechanics and Molecular Physics **6**:1–14. DOI 10.1142/S2424913021420078
[21] Russo R, Girot Mata FA, Forest S (2020) Thermomechanics of cosserat medium: Modeling adiabatic shear bands in metals, Continuum Mechanics and Thermodynamics. DOI 10.1007/s00161-020-00930-z
[22] deBorst R (1993) A generalization of J_2-flow theory for polar continua, Computer Methods in Applied Mechanics and Engineering **103**: 347–362. DOI 10.1016/0045-7825(93)90127-J
[23] Besson J, Foerch R (1997) Large scale object–oriented finite element code design, Computer Methods in Mechanical Engineering **142**:165–187.
[24] Hirth J, Lothe J (1982) Theory of Dislocations, Wiley Intersciences.

[25] Mesarovic S, Forest S, Zbib H (Eds) (2019) Mesoscale Models. From Micro-Physics to Macro-Interpretation, Springer, CISM International Centre for Mechanical Sciences, Vol 587. DOI 10.1007/978-3-319-94186-8

[26] Ask A, Forest S, Appolaire B, Ammar K, Salman OU (2018) A Cosserat crystal plasticity and phase field theory for grain boundary migration, Journal of the Mechanics and Physics of Solids **115**:167-194. DOI https://doi.org/10.1016/j.jmps.2018.03.006

[27] Fried E, Gurtin M (1993) Continuum theory of thermally induced phase transitions based on an order parameter, Physica D **68**:326–343.

[28] Gurtin M (1996) Generalized Ginzburg–Landau and Cahn–Hilliard equations based on a microforce balance, Physica D **92**:178–192.

[29] Warren JA, Kobayashi R, Lobkovsky AE, Carter W (2003) Extending phase field models of solidification to polycrystalline materials, Acta Materialia **51**:6035–6058.

[30] Lobkovsky AE, Warren JA (2001) Sharp interface limit of a phase-field model of crystal grains, Physical Review E **63**:051605.

[31] Giga MH, Giga Y (1998) Evolving graphs by singular weighted curvature, Arch Rational Mech Anal **141**:117–198. DOI 10.1007/s002050050075